https://doi.org/10.5194/acp-2019-743
Preprint. Discussion started: 2 December 2019

Atmospheric Chemistry and Physics Discussions

Influence of Asian Summer Monsoon Anticyclone on the Trace gases and Aerosols over Indian region

Ghouse Basha[1], M. Venkat Ratnam[1], Pangaluru Kishore[2], S. Ravindrababu[3] and Isabella Velicogna[2]

[1]National Atmospheric Research Laboratory, Department of Space, Gadanki-517112, India.

[2] Department of Earth System Science, University of California, Irvine, CA, 92697, USA.

[3]Center for Space and Remote Sensing Research, National Central University, No. 300, Jhongda Rd.,Jhongli Dist., Taoyuan City 32001, Taiwan

Correspondence to: Ghouse Basha (mdbasha@narl.gov.in)

Abstract

The Asian Summer Monsoon Anticyclone (ASMA) persisting during monsoon season in the upper troposphere and lower stratosphere (UTLS) region play an important role in confining the trace gases and aerosols for a longer period thus affects regional and global climate. Our understanding on these trace gases and aerosols variability in the ASMA is limited. In this study, the effect of the ASMA on the trace gases (Water Vapour (WV), Ozone (O_3), Carbon Monoxide (CO)) and aerosols (Attenuated Scattering Ratio (ASR)) obtained from long-term (2006-2016) satellite measurements is investigated. Since the ASMA is present in the UTLS region, its influence on the tropopause characteristics is also explored. Higher tropopause altitude, WV, CO and ASR confining to the ASMA region is observed, whereas tropopause temperatures and O_3 are found low. There exists large inter-annual variation in the ASMA and hence its effect on these trace gases and aerosols are also seen clearly. A significant relationship is also observed between the phases of Quasi-Biannual Oscillation (QBO) and El Niño Southern Oscillation (ENSO) on the trace gases and ASR, including the tropopause when measurements in the ASMA region are subject to multivariate regression analysis. Further, the influence of the Indian summer monsoon (ISM) activity on the ASMA trace gases and aerosols is studied with respect to active and break spells of

https://doi.org/10.5194/acp-2019-743
Preprint. Discussion started: 2 December 2019

monsoon, strong and weak monsoon years, strong La Niña, El Niño years. Results show a significant increase in WV, CO and decrease in O_3 during the active phase of the ISM, strong monsoon years and strong La Niña years in the ASMA. Enhancement in the ASR values during the strong monsoon years and strong La Niña years is observed. Thus, it is prudent to conclude that the dynamics of the ASMA play an important role in the confinement of several trace gases and aerosols and suggested to consider the activity of summer monsoon while dealing with them at sub-seasonal scales.

Keywords: Anticyclone, Monsoon, ENSO, QBO, Temperature, water vapour, ozone.

1. Introduction

The Asian Summer Monsoon Anticyclone (ASMA) is one of the dominant circulation patterns in the Northern Hemisphere (NH) Upper Troposphere and Lower Stratosphere (UTLS) region persisting during summer and has a significant influence on the global atmospheric circulation (Randel and Jensen, 2013). The ASMA is bounded by a westerly jet to the north and an easterly jet to the south and is prominent for a long duration of air confinement (Dunkerton, 1995). The features of the ASMA were studied extensively in recent years (Hoskins and Rodwell, 1995; Highwood and Hoskins, 1998; Liu et al., 2009; Wu et al., 2012). This anticyclone was identified as transport pathway for stratosphere-troposphere exchange (STE) during summer into the lower-most stratospheric layer and into the upper branch of Brewer-Dobson Circulation (BDC), particularly with regard to water vapour (WV) and pollutants (Vogel et al., 2016; Ploeger et al., 2017). Recent studies have shown the build-up of aerosols near the tropopause in the anticyclone region by the Asian monsoon circulation known as the 'Asian Tropopause Aerosol Layer (ATAL)' (Vernier et al., 2011; Vernier et al., 2018). This layer causes significant regional radiative forcing, which further causes cooling of Earth's surface and is, therefore important for a more detailed assessment of climate change.

The ASMA is characterized by persistent deep convection over the Bay of Bengal (BoB), North India and the South China Sea (Tzella and Legras, 2011; Wright et al., 2011; Bergman et al., 2012), elevated surface heating over the Tibetan Plateau (Fu et al., 2006), and orographic uplifting at the southern/south-western slopes of the Himalayas, which contribute to an overall ascension of air to higher altitudes (up to ~200 to 100 hPa). The upward transport from convective outflow to higher altitudes involves a vertical conduit over the Southern Tibetan Plateau (Bergman et al., 2013). The ASMA spans from the Middle East to East Asia (Basha et al., 2019). Due to the influence of deep convection and long-range transport, the air reached to the anticyclone will be confined and the chemical composition and tracers such as carbon monoxide (CO), WV, and Ozone (O_3) near the tropopause display distinct characteristics. In addition, the location and shape of the ASMA vary at different time scales i.e. inter-seasonal, inter-annual and longer time scales (Pokhrel et al., 2012). The ASMA varies at sub-seasonal time scales although it is strong and steady seasonal phenomena (Luo et al., 2018). The sub-seasonal dynamical processes play a vital role in transporting trace gases from the surface to the UTLS region (Garny and Randel, 2016; Pan et al., 2016).

It is well known that air enters into the ASMA region through deep convection or upwelling processes from head BoB or the South China Sea. The tropopause temperature controls the lower stratospheric (LS) WV with dehydration processes (Fueglistaler et al., 2009; Fueglistaler & Haynes, 2005; Ding & Fu, 2017). Thus, the temperature at the tropopause plays a crucial role in controlling the WV and other trace gases transport into the LS and also (cirrus) cloud formation. In addition, the tropopause temperature is highly variable, which results from the combination of Quasi-Biennial Oscillation (QBO),

https://doi.org/10.5194/acp-2019-743
Preprint. Discussion started: 2 December 2019

convective processes, and BDC circulation (Ding & Fu, 2017). It is evident that diagnosing the seasonal variability of tropopause altitude/ temperature and its relation with tracers is important for a broader understanding of the dynamical impacts of the anticyclone. Thus, this study aims to bridge the gap with the help of long-term observations of tropopause altitude, temperature from the Global Position System (GPS) Constellation Observing System for Meteorology, Ionosphere, and Climate (COSMIC) data, WV mixing Ratio (WVMR), O_3, CO from the Microwave Limb Sounder (MLS) satellite, and Attenuated Scattering Ratio (ASR) from the Cloud-Aerosol Lidar and Infrared Pathfinder Satellite Observations (CALIPSO) Stratospheric aerosol product in the ASMA region.

In this study, we investigate the climatology, seasonal and inter-annual variability of the trace gases, as well as the variability of these parameters with respect to QBO and the El Niño–Southern Oscillation (ENSO) (La Niña and El Niño) within the ASMA. Further, the variability of tropopause temperature, altitude, trace gases, and ASR spatial variability is studied with respect to active and break spells of ISM, strong and weak monsoon years and strong ENSO years. This paper is structured as follows: Section 2 provides a description of the different data used for the present study. In section 3, the climatology and inter-annual variation of the tropopause altitude, temperature, WVMR, O_3, CO and ASR during the period 2006-2016 are discussed. In Section 4, the influence of Indian monsoon on the spatial variability of tropopause parameters and tracers, ASR are presented. Finally, summary and discussion are provided in Section 5.

2. Data base

2.1. COSMIC GPS RO measurements

To identify the tropopause parameters, we have utilized COSMIC GPS RO satellite measurements. COSMIC consist of a constellation of 6 satellites which was launched in April 2006 to a circular, 72° inclination orbit at a 512 km altitude capable of receiving signals from

https://doi.org/10.5194/acp-2019-743
Preprint. Discussion started: 2 December 2019

GPS (Anthes et al., 2008). Compared to previous satellites, COSMIC satellites employed an open-loop mode, which can track both the set and rise of occultations (Schreiner et al. 2007). The open-loop tracking technique significantly reduces the GPS radio occultation inversion biases by eliminating tracking errors (Sokolovskiy et al. 2006). This receiver measures the phase delay of radio wave signals that are occulted by the Earth's atmosphere. From this phase delay, it is possible to retrieve the bending angle and refractivity profiles. From refractivity profiles, profiles of temperature can be derived with an accuracy of <0.5 K (Kursinski et al., 1997). The COSMIC temperature profiles showed very good agreement with radiosonde data, reanalysis, and models (Rao et al., 2010; Ratnam et al., 2014; Kishore et al., 2016). In this article, we derived the Cold Point Tropopause (referred as tropopause altitude and tropopause temperature throughout the paper) over the ASMA region as discussed by and Ratnam et al. (2014) and Ravindrababu et al. (2015).

2.2. Microwave Limb Sounder (MLS) measurements

For understanding the trace gases distribution in the ASMA, we make use of MLS measurements. The MLS uses the limb sounding technique for measuring WVMR, O_3, CO, and other tracers in the UTLS region. This satellite was launched in August 2004 onboard the Aqua spacecraft as a part of NASA's Earth Observing Systems (EOS). The MLS scans limb vertically in the orbit plane and gives a latitude coverage ranging from 82^{o}S to 82^{o}N. We used version 4.2 MLS data of WVMR, O_3, and CO mixing ratios obtained from the Mirador website (https://disc.gsfc.nasa.gov/). MLS WV has a precision of 0.4 ppmv at 100 hPa for individual profile measurements, with a spatial scale of 200 km along the line of sight (Schwartz et al., 2013). The vertical resolution of the water vapour product is 3 km in the lower stratosphere (Livesey et al., 2015). The O_3 retrieval has a vertical resolution of 3 km at 100 hPa. The precision and accuracy are ~30 ppbv and ~50 ppbv, respectively (Livesey et al., 2015). The root mean square average of the estimated precision of CO has a root mean square

https://doi.org/10.5194/acp-2019-743
Preprint. Discussion started: 2 December 2019

precision of 20 ppbv at 100 hPa with a possible bias of ±20 ppbv. More details about MLS version 4.2 data can be found in Livesey et al. (2018). We constructed gridded daily data by averaging profiles inside bins with a resolution of 5° latitude × 5° longitude.

2.3. Cloud-Aerosol Lidar and Infrared Pathfinder Satellite Observations (CALIPSO) Stratospheric Aerosol Profile

For understanding the aerosol distribution in the ASMA region, we considered the CALIPSO measurements. The CALIPSO satellite was a part of the A-train constellation, which was launched in April 2006 to a Sun Synchronous polar orbit 98.2° inclination at an altitude of 705 km (Winker et al., 2009). The constellation repeats the cycle every 16 days with local equator crossing times of nearly 01:30 h and 13:30 h (Winker et al., 2009). The Cloud-Aerosol Lidar with Orthogonal Polarization (CALIOP) was one of the main instruments on board the CALIPSO satellite with a dual-wavelengths (532 nm and 1,064 nm) polarization sensitive lidar. CALIOP provides profiles of clouds and aerosols and is capable of detecting clouds with an optical depth of 0.01 or less. We utilized level 3 global distribution of monthly gridded stratospheric aerosol profile data of 532 nm ASR (https://eosweb.larc.nasa.gov/project/calipso/cal_lid_l3_stratospheric_apro-standard_v1-00). This profile data is available on a monthly basis with 900 m vertical resolution from 8.2 km to 36.2 km in the tropical latitudes.

Apart from these datasets we also used normalized zonal winds at 30 hPa from Singapore's radiosonde observations for the QBO index, the multivariate ENSO index (https://www.esrl.noaa.gov/psd/enso/mei/) as well as geopotential height (GPH), zonal, and meridional winds at 100 hPa from National Centers for environmental Prediction (NCEP) and the National Center for Atmospheric Research (NCAR) reanalysis data.

https://doi.org/10.5194/acp-2019-743
Preprint. Discussion started: 2 December 2019

3. Methodology

To quantify the contribution of QBO and ENSO to the tropopause parameters, tracers and on aerosols data are subjected to the multivariate regression analysis. This well-established method considers the relative influence of the considered climate indices on tropospheric variability. For more details about the regression technique and its further applications see Diallo et al. (2012; 2017). The regression technique is expressed as:

$$res(t) = a_1 + a_2(t) + a_3 \, Sin(2\pi t) + a_4 \, Cos(2\pi t) + a_5 \, Sin(4\pi t) + a_6 \, Cos(4\pi t) + a_7 \, .QBO(t) + a_8 \, . ENSO\,(t) + \varepsilon(t) \quad (1)$$

where $a_1(t)$ to $a_8(t)$ are coefficients, QBO(t) and ENSO(t) the normalized QBO time-series represented by the biennial modulations of the monthly mean zonal winds at 10 hPa (~30 km altitude) measured by radiosonde in Singapore and normalized-Nino 3.4 (ENSO) index, $\varepsilon(t)$ is random noise. With these coefficients, we have estimated the amplitude changes associated with interannual cycles.

4. Results and Discussion

4.1. Climatological state of the of anticyclone during the summer monsoon

It is well reported that the ASMA will be fully covered and active over the entire monsoon region (15°-45°N and 0°-130°E) in the months of July and August (Ju and Slingo, 1995; Santee eta al., 2017; Basha et al., 2019). In this study, we have also considered similar month average for studying the ASMA. The climatological GPH superimposed with wind vectors at 100 hPa from NCEP/NCAR reanalysis data during July, August months from 2006 to 2016 is shown in Figure 1. A strong anticyclonic flow is evident from the figure which lies between ~22.5°-40°N and 30°-120°E in the Northern Hemisphere (NH). The area with the highest GPH (in red) displays the ASMA region. The intensity of the anticyclone is large exactly over the Tibetan Plateau. The climatological mean spatial distribution of tropopause altitude, the tropopause temperature from COSMIC, WVMR, O_3, and CO from MLS at 100

https://doi.org/10.5194/acp-2019-743
Preprint. Discussion started: 2 December 2019

hPa and the ASR from CALIPSO averaged in the range of 16-18 km along with wind vectors at 100 hPa from NCEP during July and August are shown in the Figure 2 averaged for the period 2006-2016. The white line shows the 16.75km GPH value at 100 hPa, which represents the core of the anticyclone. Higher tropopause altitude, WVMR, and CO and lower tropopause temperature and O_3 are evident within ASMA from Figure 2. Enhancement in ASR is also observed in the anticyclone region. Globally the highest tropopause altitude is observed over the ASMA region and this is balanced by a dynamical structure tied to the strong anticyclonic circulation (Hoskins et al., 1985). The height of the tropopause reaches ~18-18.5 km in the northwest of the ASMA region. The strong convection leads to colder tropopause temperatures in the anticyclone region and in the subtropical lower stratosphere. It is reported that, cold tropopause temperatures leads to frequent dehydration and these contribute to decoupling water vapour and the other tracers (Park et al., 2007). WV increases broadly at 100 hPa in the anticyclone region during the summer monsoon (referred to July and August in this study) as shown in Figure 2c. A large amount of WV is located over north-east of the anticyclone i.e. over the Tibetan Plateau. Relatively high WV is transported through deep convection from BoB and the Indian Ocean (Basha et al., 2019). Within the anticyclone, CO has a broad maximum towards the south-west of the anticyclone which coincides with the strong horizontal circulation between 20^o to 120^{o}E longitude. The upper tropospheric anticyclone has a distinct signature of tracers such as CO, which have near-surface sources (from combustion) and is thought to be transported upward by deep convection associated with the monsoon (Randel et al., 2015). This deep convection significantly alters CO, $O_{3,}$ and WV near the tropopause region. These observations clearly show higher values of CO, and low values of O_3 transported from the troposphere through deep convection associated with the monsoon (Randel et al., 2015). It is well reported that, higher (lower) values of CO (O_3) in the anticyclone are result of strong tropospheric

https://doi.org/10.5194/acp-2019-743
Preprint. Discussion started: 2 December 2019

Atmospheric Chemistry and Physics
Discussions

(stratospheric) tracers (Ploeger et al., 2015). Rich O_3 and poor CO air will be advected to the extra-tropical stratosphere through the eastern flank of anticyclone towards the equator (Ploeger et al., 2015). The higher tropopause attitudes, a large amount of WVMR, CO with low O_3 are centred within the ASM anticyclone. Figure 2f shows the climatological mean ASR averaged in the range of 16-18 km altitude from 2006 to 2016 for July and August months superimposed with wind vectors at 100 hPa. These observations clearly indicate the presence of enhanced aerosols in the anticyclone region with ASR magnitude ranging from 1-1.5. These large amounts of aerosol are seen in the middle and western part of the anticyclone.

Figure 3 shows the monthly mean vertical variation of UTLS temperatures, WVMR, O_3, CO, and ASR averaged over the anticyclone region (area under the white line in Figure 2; In the grid of 30°E-110° E longitude and 22.5°N-40°N latitude) for the period 2006-2016, superimposed with tropopause altitude. Significant seasonal variability is observed in all the parameters. Coldest temperatures are observed in the range of 16-18 km in all the months. During July and August months very low temperatures are observed compared to other months where highest tropopause altitude is observed. Similar variation is observed in O_3 a higher concentration of WVMR and CO is observed July and August months. The seasonal cycle of the tropopause which is higher during monsoon matches precisely with tracers variations. Tropopause altitude starts increasing from the month of April and reaches its peak in August, whereas temperature starts decreasing in April and reaches a minimum in July. The lowest tropopause temperatures are observed exactly above the tropopause altitude during June-July whereas WVMR shows a peak during August. Further, O_3 reaches its minimum in September. In the case of CO, the peak is observed during July. The tropopause altitude and WV shows a maximum during August whereas $O_3$is lowest during September. One month delay is observed between WVMR and O_3. The most striking feature is the tape recorder effect in the stratosphere is also noticed in the anticyclone region. The observations of enhanced aerosol above the tropopause clearly indicates that ait enter into the lower stratosphere through the anticyclone region. This is the direct evidence for increase in aerosols above the tropopause in the ASMA region. The major pathway for the transport of aerosols to the lower stratosphere is thought to be due to deep convection (Chakraborty et al. 2015). In the ASMA region, ~70% of stratospheric aerosols originate from lower-tropospheric SO_2 and organics, with roughly equal contributions from within the ASMA and from the tropics (Fadnavis et al., 2013).

Figure 4 shows the interannual variation in temperature, WVMR, O_3, CO, ASR averaged in the anticyclone region along with the volcanic explosivity index (VEI). The lowest values in temperature are observed between 16 and 18 km in the anticyclone region. Both the temperature and tropopause altitude shows significant inter-annual variation. This variation is much more pronounced in WVMR, O_3, and CO. There is a clear relationship between the tropopause altitude and other tracers in the anticyclone region. The tape recorder effect is clearly observed in the inter-annual variation of WV obtained from MLS data in the anticyclone region, which represents large-scale upward transport (Mote et al., 1996). The peak values of ASR are observed during July and August every year. On 7August 2008, volcanic aerosols were transported towards Asia due to volcanic eruption from Okmok. Large values of ASR are found during the years 2009 where a large plume of 1 Tg of SO_2 was ejected into the lower stratosphere after the eruption of Sarychev volcano (Russia) on 7 June 2009 (Haywood et al., 2010). Similarly, in 2011, Nabro a stratovolcono in northeast Africa erupted on 12 June 2011; these signals are also observed in the inter-annual variation of ASR. Irrespective of these volcanoes, the Asian Tropopause Aerosol Layer (ATAL) is present in all the years. This was supported by the VEI which is a measure of explosiveness of volcanic eruption (Figure 4f). At interannual time scales, the tropopause altitude correlates highly with

https://doi.org/10.5194/acp-2019-743
Preprint. Discussion started: 2 December 2019

O_3 (-0.95), WVMR (0.92), CO (0.90) and ASR (0.44) and with tropopause temperature vice versa. WVMR correlates highly with O_3 (-0.93), CO (0.62) and ASR (0.47). Similarly, O_3 correlated significantly with CO (-0.82) and ASR (-0.38). Finally, CO and ASR have a correlation coefficient of 0.48. The tropopause parameters and tracers are highly correlated to one another in the anticyclone region. The lag-lead correlation between tropopause altitude and WVMR and O_3 is zero, whereas it has a lag of 1 month for CO and ASR. The same analysis for tropopause temperature shows that WVMR exhibits a 1-month lead, O_3 and CO shows no lag and ASR has a 1-month lag. Further, cross wavelet and wavelet coherence analyses between tropopause altitude and WVMR, CO, ASR shows in-phase relation whereas O_3 represents anti-phase relation and vice-versa for tropopause temperature and tracers.

4.2. Influence of QBO and ENSO

So far we have discussed the spatial and temporal variability of tropopause parameters, tracers, and aerosols within the ASMA. Here, we distinguish the significant internal modes of inter-annual variability such as the QBO and ENSO. We made an attempt to separate the influences of QBO and ENSO in the anticyclone region. Figures 5 and 6 show the deseasonalized time series of tropopause temperature, altitude, WVMR, O_3, and CO at 100 hPa, as well as the averaged ASR in the range of 16-18 km obtained with multivariate regression analysis based on QBO (Singapore zonal wind at 30 hPa) and ENSO proxies, respectively (Randel et al., 2015). The QBO and ENSO data is also plotted on the right side of the plot. The resulting data captures the inter-annual variability of all the parameters in the anticyclone region as shown in Figure 5 and 6. Higher (lower) values of tropopause altitude and CO correspond to the eastward (westward) phase of the QBO. The opposite is true in cases of tropopause temperature and O_3. The westward (eastward) phase of the QBO matches with higher (lower) WV values at 100 hPa. The positive values of ASR correspond to the eastward phase of QBO and vice versa.

https://doi.org/10.5194/acp-2019-743
Preprint. Discussion started: 2 December 2019

Similarly, higher (lower) values of tropopause altitude, WVMR, CO, and ASR correspond to El Niño (La Niña) conditions over the anticyclone, whereas tropopause temperature and O_3 show the opposite pattern (Figure 6). Previous studies have also shown the transport of WV during La Niña conditions to the UTLS region in the Western Pacific (Randel et al., 2015). Further, a lag-lead difference is observed between the QBO and the regression coefficients obtained for all the parameters. The influence of the QBO is seen clearly in the anticyclone region. In addition, Empirical Mode decomposition (EMD) analysis is also performed on the all parameters, yielding a set of Intrinsic Mode Functions (IMFs). Lomb Scale Periodogram (LSP) analysis applied to the IMFs shows that seasonal, annual, QBO and ENSO components are the significantly dominant modes in all parameters.

4.3. Influence of Indian summer monsoon activity

It is well known that Indian monsoon rainfall varies at different time scales i.e. daily, sub-seasonal, inter-annual, decadal and centennial scales. Precipitation during monsoon varies from intra-seasonal scales between active (high rainfall) and break (low rainfall) spells. Any small change in the precipitation pattern will affect the tracer composition in the anticyclone due to thermodynamics involved in the rainfall. In this study, we also investigated the anticyclone variability during active and break spells of the Indian monsoon. The active and break spells were identified for July and August by using high resolution gridded (0.25^o x 0.25^o) rainfall data from 2006 to 2016 as defined by Rajeevan et al. (2010). Figure 7 shows the spatial difference between active and break day's variability in the tropopause altitude, temperature, WVMR, O_3, and CO. The black color line indicates the 16.75 km GPH which represents the anticyclone region. The tropopause altitude increases slightly whereas temperature decreases during the active phase of the monsoon. The WVMR depicts a significant increase in the anticyclone region whereas O_3 shows a quite opposite

https://doi.org/10.5194/acp-2019-743
Preprint. Discussion started: 2 December 2019

Atmospheric Chemistry and Physics Discussions

picture which is expected. The CO shows a slight increase during the active days of monsoon.

In a similar way, we have separated the strong and weak monsoon years based on gridded precipitation data from 2006 to 2016. We have chosen the domain (5-30^{o}N, 70-95^{o}E) to identify the strong and weak monsoon years. This region receives a large amount of precipitation and subjected orographic forcings, which helps the transport of WV to the UTLS region through deep convection. The mean precipitation over the selected domain during July and August subjected to de-trend analysis shows the strong inter-annual variability. The strong (weak) monsoon years were identified where rainfall was above (below) the 1 standard deviation. The strong (weak) monsoon years were 2010, 2011, 2013 (2014, 2015). The spatial difference between strong and weak monsoon years in all the parameters is shown in Figure 8. In the anticyclone region, the tropopause altitude and temperature shows a moderate increase and decrease, respectively, but these changes are not significant. The WVMR, CO, and O_3 show significant changes in the anticyclone region. The WVMR and CO increases significantly during the strong monsoon years where O_3 decreases. Increase in ASR is noticed over the north of the anticyclone region. It is noticed that aerosols are confined to NH in the latitude band of 30^o-40^{o}N and the peak coincides with the anticyclone.

Further, tropopause parameters, tracers, ASR have been separated for strong La Niña (2007, 2010) and El Niño (2015) years and the resultant difference between La Niña and El Niño composite plot is shown in Figure 9. The strong ENSO years are selected from the website https://ggweather.com/enso/oni.htm. The increase (decrease) in tropopause altitude (temperature) is clearly noticed from Figure 9 (a & b). These changes are not clearly observed in active and break phase of Indian monsoon, strong and weak monsoon years. The significant increase in WVMR, CO, and decrease in O_3 is large compared to the previous

https://doi.org/10.5194/acp-2019-743
Preprint. Discussion started: 2 December 2019

discussion. The ASR also increases during the strong La Niña months compared to El Niño. The enhanced aerosols represent the transport above the tropopause altitude and suggest that air enter the stratosphere within the anticyclone region during La Niña and strong monsoon years. Previous studies also suggested that pollutants could be transported to higher altitude through deep convection (Park et al., 2009; Randel et al., 2010). Aerosol transport is large over South Asia during the deep convection as suggested by Chakraborty et al. (2015). It is well known that deep convection occurs most frequently over the BoB and the Indian subcontinent during monsoon and a large amount of WVMR and CO and low O_3 through convection processes in the upper troposphere. Thus, the activity of the monsoon also plays an important role on the ASMA and hence on its tracers and aerosol distribution.

5. Summary and Conclusions

In this study, we have investigated the influence of the ASMA on the temporal and spatial variability of tropopause temperature/altitude, tracers (WV, O_3, CO) and aerosol from COSMIC, MLS and CALIPSO satellite data sets obtained during 2006 to 2016. Further, with the help of these observational datasets, we carried out an in-depth analysis to find the relation between the ASMA and QBO and ENSO. The main highlights of the present study are summarized below.

1. Higher tropopause altitude, WVMR, CO, and ASR and lower tropopause temperature and O_3 are noticed in the ASMA region during July and August months.
2. Lower temperatures are located exactly above the tropopause altitude in the ASMA. The low (high) concentrations of O_3 (CO) are located below the tropopause. Similar features are observed in the inter-annual variation of temperature, and in other tracers.
3. The ASR is very high in the altitude range of 16.5-18.5 km in the ASMA region. Enhancement in ASR is found during the year 2008, 2009, and 2011 where major volcanic eruptions occurred but not always related to these eruptions.

https://doi.org/10.5194/acp-2019-743
Preprint. Discussion started: 2 December 2019

4. The estimated correlation coefficients indicate good to a fair agreement among tropopause parameters, tracers, and aerosols.
5. The deseanonalized time series subjected to multivariate regression analysis shows a higher (lower) tropopause altitude and CO corresponding to the eastward (westward) phase of the QBO. The opposite is true in cases of tropopause temperature and O_3. The westward (eastward) phase of the QBO matches with higher (lower) WVMR at 100 hPa. Enhancement in ASR is observed during the eastward phase of QBO and vice versa in the ASMA region.
6. Similarly, higher (lower) tropopause altitude, WVMR, CO, and ASR is observed in La Niña (El Niño) conditions over the anticyclone, whereas tropopause temperature and O_3 show the opposite pattern.
7. A significant influence of ISM activity on the spatial variability of tropopause temperature/altitude, tracers and ASR is found. In ASMA, enhancement in WVMR, CO and decrease in O_3 are observed during active phase of Indian monsoon, strong monsoon years and during strong La Niña years. The ASR is large during the strong monsoon years and during strong La Niña years in ASMA region.
8. A significant increase (decrease) in tropopause altitude (temperature) is observed during strong La Niña and these features are not clearly depicted during the active/break, strong/weak monsoon years in ASMA region.
9. Our findings demonstrated that the tracers and aerosols in the ASMA are significantly impacted by the transport processes of moisture and pollutants from the northern part of Tibetan Plateau.

Overall, we have shown that the Asian summer monsoon circulation plays an important role in determining the mean pattern and variability of the tropopause, tracers, and ASR, providing a useful framework for studying the underlying mechanisms. The mechanism of

WV and CO transport into the lower stratosphere in this region is an important aspect towards understanding the tropospheric influences on the hydration and chemical composition in the global stratosphere. The strong correlation between the tropopause and WVMR during the monsoon season is due to zonally asymmetric surface heating associated with the summer monsoon. Deep convection (i.e., thunderstorm updrafts) occurs most frequently over the BoB and the Indian subcontinent. Strong convection occurs both directly below the Asian monsoon anticyclone in India and China and outside the anticyclone region over Southeast Asia and the Pacific Ocean. Deep convection and a conduit of upwelling air over the Tibetan plateau (Bergman et al., 2013) inject lower-tropospheric air mainly into the Tibetan part of the ASMA. Further during strong monsoon, the tracers are transported from Himalayas Gangetic Plain and the Sichuan Basin into the ASMA. These tracers are adverted by the ASMA circulation which results in large spatial distribution of tracers (Yuan et al., 2019). The control of tropopause parameters, tracers and aerosols depend on the interactions of ENSO events and QBO Phases. It is clear that ENSO impacts both tropopause height and temperature. Enhanced CO is an indicator of this process. Lelieveld et al. (2018b) and Vernier et al. (2018) showed emissions and transport of dust aerosols into the ASMA from the north part of the Tibetan Plateau and this will acts as a well-defined conduit for transport processes. The interaction of these natural and anthropogenic aerosols and gases in the ASMA need further investigations. Further, aerosol effects on the monsoon water cycle may be important in years when influence from other controlling factors (sea surface temperature, land surface processes, and internal dynamics) which will additionally affect the ASMA region. The enhancement in ASR can modify the radiation in the UTLS region which will affect the heating rates inside the anticyclone and are significantly larger than those surrounding areas which will be carried out in the future.

*Data Availability***.** The NCEP/NCAR reanalysis data are available from NOAA website (https://www.esrl.noaa.gov/psd/data/gridded/data.ncep.reanalysis.pressure.html). The COSMIC data is available from COSMIC CDAAC website. MLS data obtained from Earth Science Data website. CALIPSO stratospheric aerosol product is obtained from Atmospheric Science Data Center. IMD gridded precipitation data is available at National Climate data center Pune, India. All the data used in the present study is available freely from the respective websites.

Authors 'Contributions. GB and MVR conceived and designed the scientific questions investigated in the study. GB performed the analysis and wrote the draft in close cooperation with MVR. RB and PK estimated the active and break spells of the Indian monsoon. All authors edited the paper.

Competing Interests. The authors declare that they have no competing financial interests.

Acknowledgements. We thank NCEP/NCAR reanalysis for providing reanalysis data. We thank CDAAC for production of COSMIC GPSRO data, MLS data through Earth science data CALIPSO stratospheric aerosol data from atmospheric science data center, NASA and IMD gridded precipitation data from National Climate data center Pune, India. This work was supported by National Atmospheric Research Laboratory, Department of Space, and India

References

Anthes, R., Bernhardt, P., Chen, Y., Cucurull, L., Dymond, K., Ector, D., Healy, S., Ho, S., Hunt, D., Kuo, Y., Liu, H., Manning, K., Mccormick, C., Meehan, T., Randel, W., Rocken, C., Schreiner, W., Sokolovskiy, S., Syndergaard, S., Thompson, D., Trenberth, K., Wee, T., Yen, N., and Zeng, Z.: The COSMIC/FORMOSAT-3 – Mission early results, B. Am. Meteorol. Soc., 89, 313–333, 2008.

Basha, G., Ratnam, M. V., and Kishore, P.: Asian Summer Monsoon Anticyclone: Trends and Variability, Atmos. Chem. Phys. Discuss., https://doi.org/10.5194/acp-2019-668, in review, 2019.

Bergman, J. W., Fierli, F., Jensen, E. J., Honomichl, S., and Pan, L. L.: Boundary layer sources for the Asian anticyclone: Regional contributions to a vertical conduit, J. Geophys. Res., 118, 2560–2575, https://doi.org/10.1002/jgrd.50142, 2013.

Bergman, J. W., Jensen, E. J., Pfister, L., and Yang, Q.: Seasonal differences of vertical-transport efficiency in the tropical tropopause layer: On the interplay between tropical deep convection, largescale vertical ascent, and horizontal circulations, J. Geophys. Res., 117, D05302, https://doi.org/10.1029/2011JD016992, 2012.

Chakraborty, S., Fu, R., Wright, J. S., and Massie, S. T.: Relationships between convective structure and transport of aerosols to the upper troposphere deduced from satellite observations, J. Geophys. Res. Atmos., 120, 6515–6536, doi:10.1002/2015JD023528, 2015.

Diallo, M., Legras, B., and Chédin, A.: Age of stratospheric air in the ERA-Interim, Atmos. Chem. Phys., 12, 12133–12154, https://doi.org/10.5194/acp-12-12133-2012, 2012.

Diallo, M., Ploeger, F., Konopka, P., Birner, T., Müller, R., Riese, M., Garny, H., Legras, B., Ray, E., Berthet, G., and Jegou, F.: Significant contributions of volcanic aerosols to decadal changes in the stratospheric circulation, Geophys. Res. Lett., 44, 10780– 10791, https://doi.org/10.1002/2017GL074662, 2017.

Ding, Q., and Fu, Q.: A warming tropical central Pacific dries the lower stratosphere, Clim.Dyn., https://doi.org/10.1007/s00382-017-3774-y, 2017.

Dunkerton, T. J.: Evidence of meridional motion in the summer lower stratosphere adjacent to monsoon regions, J. Geophys. Res., 100, 16,675 – 16,688, 1995.

Fischer, H., Wienhold, F. G., Hoor, P., Bujok, O., Schiller, C., Siegmund, P., Ambaum, M., Scheeren, H. A., and Lelieveld, J.: Tracer correlations in the northern high latitude lowermost stratosphere: Influence of crosstropopause mass exchange, Geophys. Res. Lett., 27, 97 – 100, 2000.

Fu, R., Hu, Y., Wright, J. S., Jiang, J. H., Dickinson, R. E., Chen, M., Filipiak, M., Read, W. G., Waters, J. W., and Wu, D. L.: Short circuit of water vapour and polluted air to the global stratosphere by convective transport over the Tibetan Plateau, P. Natl. Acad. Sci. USA, 103, 5664–5669, 2006.

Fueglistaler, S., Bonazzola, S., Haynes, P. H., and Peter, T.: Stratospheric water vapor predicted from the Lagrangian temperature history of air entering the stratosphere in the tropics, J. Geophys. Res., 110, 8107, doi:10.1029/2004JD005516, 2005.

Fueglistaler, S., Dessler, A. E., Dunkerton, T. J., Folkins, I., Fu, Q., and Mote, P. W.: Tropical Tropopause Layer, Rev. Geophys., 47, RG1004, doi:10.1029/2008RG000267., 2009.

Garny, H., and Randel, W. J.: Transport pathways from the Asian monsoon anticyclone to the stratosphere, Atmos. Chem. Phys., 16, 2703–2718, https://doi.org/10.5194/acp-16-2703-2016, 2016.

Highwood, E. J., and Hoskins, B. J.: The tropical tropopause, Q. J. Roy. Meteorol. Soc., 124, 1579–1604, 1998.

Hoor, P., Fischer, H., Lange, L., Lelieveld, J., and Brunner D.: Seasonal variations of a mixing layer in the lowermost stratosphere as identified by the CO-O3 correlation from in situ measurements, J. Geophys. Res., 107(D5), 4044, doi:10.1029/2000JD000289, 2002.

Hoskins, B. J. and Rodwell, M. J.: A model of the Asian summer monsoon. Part I: the global scale, J. Atmos. Sci., 52, 9, 1329– 1340, 1995.

https://doi.org/10.5194/acp-17-7055-2017, 2017.

Ju, J., and Slingo, J.: The Asian summer monsoon and ENSO, Q. J. R. Meteorol. Soc., 121, 1133– 1168, 1995.

https://doi.org/10.5194/acp-2019-743
Preprint. Discussion started: 2 December 2019

Kishore P et al: Evaluating CMIP5 models using GPS radio occultation COSMIC temperature in UTLS region during 2006–2013: Twenty-first century projection and trends. ClimDyn. https ://doi. org/10.1007/s0038 2-016-3024-8, 2016.

Kursinski, E. R., Hajj, G. A., Schofield, J. T., Linfield, R. P., and Hardy, K. R.: Observing Earth's atmosphere with radio occultation measurements using the Global Positioning System, J. Geophys. Res., 102, 23429–23465, 1997.

Li, Q., H.-F. Shi, A.-M. Shao, et al.,: Distribution and variation of carbon monoxide in the tropical troposphere and lower stratosphere, Atmos. Oceanic Sci. Lett., **7**, 218–223, doi:10.3878/j.issn.1674-2834.13.0111, 2014.

Liu, J. J., Jones, D. B. A.,Worden, J. R., Noone, D., Parrington, M., and Kar, J.: Analysis of the summertime buildup of tropospheric ozone abundances over the Middle East and North Africa as observed by the Tropospheric Emission Spectrometer instrument, J. Geophys. Res., 114, D05304, doi:10.1029/2008JD010993, 2009.

Livesey, N. J., Read, W. G., Wagner, P. A., Froidevaux, L., Lambert, A., Manney, G. L., Millán Valle, L. F., Pumphrey, H. C., Santee, M. L., Schwartz, M. J., Wang, S., Fuller, R. A., Jarnot, R. F., Knosp, B. W., and Martinez, E.: Version 4.2x Level 2 data quality and description document, Tech. Rep. JPL D-33509 Rev. A, Jet Propulsion Laboratory, available at: http://mls.jpl.nasa.gov/ data/v4-2_data_quality_document.pdf (last access: 2 September 2016), 2015.

Livesey, N.J.; Read, W.G.; Wagner, P.A.; Froidevaux, L.; Lambert, A.; Manney, G.L.; Pumphrey, H.C.; Santee, M.L.; Schwartz, M.J.; Wang, S.; et al. Aura Microwave Limb Sounder (MLS) Version 4.2× Level 2 Data Quality and Description Document; JPL D-33509 Rev.D, Tech. Rep.; NASA Jet Propulsion Laboratory, California Institute of Technology: Pasadena, CA, USA, 2018a.

https://doi.org/10.5194/acp-2019-743
Preprint. Discussion started: 2 December 2019

Lelieveld, J., Bourtsoukidis, E., Brühl, C., Fischer, H., Fuchs, H., Harder, H., Hofzumahaus, A., Holland, F., Marno, D., Neumaier, M., Pozzer, A., Schlager, H., Williams, J., Zahn, A., and Ziereis, H.: The South Asian monsoon—pollution pump and purifier, Science, 361, 270–273, https://doi.org/10.1126/science.aar2501, http://science.sciencemag.org/content/361/6399/270, 2018b.

Luo, J., Pan, L. L., Honomichl, S. B., Bergman, J. W., Randel, W. J., Francis, G., Clerbaux, C., George, M., Liu, X., and Tian, W.: Space–time variability in UTLS chemical distribution in the Asian summer monsoon viewed by limb and nadir satellite sensors, Atmos. Chem. Phys., 18, 12511–12530, https://doi.org/10.5194/acp-18-12511-2018, 2018.

Mote, P., Rosenlof, K., Mclntyre, M., Carr, E., Gille, J., Holton, J., Kinnersley, J., Pumphrey, H., Russel, J., and Waters, J.: An atmospheric tape recorder: The imprint of tropical tropopause temperatures on stratospheric water vapor, J. Geophys. Res., 101, 3989– 4006, 1996

Pan, L. L., Honomichl, S. B., Kinnison, D. E., Abalos, M., Randel, W. J., Bergman, J. W., and Bian, J.: Transport of chemical tracers from the boundary layer to stratosphere associated with the dynamics of the Asian summer monsoon, J. Geophys. Res., 121, 14159–14174, https://doi.org/10.1002/2016JD025616, 2016.

Pan, L. L., Randel, W. J., Gary, B. L., Mahoney, M. J., and Hintsa, E. J.: Definitions and sharpness of the extratropical tropopause: A trace gas perspective, J. Geophys. Res., 109, D23103, doi:10.1029/ 2004JD004982, 2004.

Park, M., Randel, W. J., Gettelman, A., Massie, S. T., and Jiang, J. H.: Transport above the Asian summer monsoon anticyclone inferred from Aura MLS tracers, J. Geophys. Res, 112, D16309, doi:10.1029/2006JD008294, 2007.

Ploeger, F., Gottschling, C., Griessbach, S., Grooß, J.-U., Günther, G., Konopka, P., Müller, R., Riese, M., Stroh, F., Tao, M., Ungermann, J., Vogel, B., and von Hobe, M.: A potential vorticitybased determination of the transport barrier in the Asian summer monsoon anticyclone, Atmos. Chem. Phys., 15, 13145–13159, doi:10.5194/acp-15-13145-2015, 2015.

Ploeger, F., Konopka, P., Walker, K., and Riese, M.: Quantifying pollution transport from the Asian monsoon anticyclone into the lower stratosphere, Atmos. Chem. Phys., 17, 7055–7066, https://doi.org/10.5194/acp-17-7055-2017, https://www.atmos-chem-phys.net/17/7055/ 2017/, 2017.

Pokhrel, S., Chaudhari, H. S., Saha, S. K., Dhakate, A., Yadav, R. K., Salunke, K., Mahapatra, S., and Rao, S. A.: ENSO, IOD and Indian Summer Monsoon in NCEP climate forecast system, Clim. Dynam., 39, 2143–2165, https://doi.org/10.1007/s00382-012-1349-5, 2012.

Randel, W. J. and Jensen, E. J.: Physical processes in the tropical tropopause layer and their roles in a changing climate, Nat. Geosci., 6, 169–176, doi:10.1038/ngeo1733, 2013.

Randel, W. J., Zhang, K., and Fu, R.: What controls stratospheric water vapor in the NH summer monsoon regions?, J. Geophys. Res.-Atmos., 120, 7988–8001, doi:10.1002/2015JD023622, 2015.

Rao, D.N., Ratnam, M.V., Mehta, S., Nath, D., Basha, G., Jagannadha Rao, V.V.M., et al: Validation of the COSMIC radio occultation data over gadanki (13. 48°N, 79.2°E): A tropical region, Terr J Atmos Ocean Sci 20, 59–70, https://doi.org/10.3319/TAO.2008.01.23.01(F3C), 2009.

Ratnam, M.V., Sunilkumar, S.V., Parameswaran, K., Murthy, B.V.K., Ramkumar, G., Rajeev, K., Basha, G., Babu, S.R., Muhsin, M., Mishra, M.K., et al.: Tropical tropopause dynamics (TTD) campaigns over Indian region: an overview, J. Atmos. Solar-Terrestrial Phys. 121, 229–239, 2014.

RavindraBabu, S., VenkatRatnam, M., Basha, G., Krishnamurthy, B. V., and Venkateswararao, B.: Effect of tropical cyclones on the tropical tropopause parameters observed using COSMIC GPS RO data, Atmos. Chem. Phys., 15, 10239–10249, doi:10.5194/acp-15-10239-2015, 2015.

Santee, M. L., Manney, G. L., Livesey, N. J., Schwartz, M. J.,Neu, J. L., and Read, W. G.: A comprehensive overview ofthe climatological composition of the Asian summer monsoon anticyclone based on 10 years of Aura Microwave LimbSounder measurements, J. Geophys. Res.-Atmos., 122, 5491–5514, https://doi.org/10.1002/2016JD026408, 2017.

Schwartz, M. J., Read, W. G., Santee, M. L., Livesey, N. J., Froidevaux, L., Lambert, A., and Manney, G. L.: Convectively injected water vapor in the North American summer lowermost stratosphere, Geophys. Res. Lett., 40, 2316–2321, doi:10.1002/grl.50421, 2013.

Sokolovskiy, S., Kuo, Y.-H., Rocken, C., Schreiner, W. S., Hunt, D., and Anthes, R. A.: Monitoring the atmospheric boundary layer by GPS radio occultation signals recorded in the open-loop mode, Geophys. Res. Lett., 33, L12813, doi:10.1029/2006GL026112, 2006.

Tzella, A., and Legras, B.: A Lagrangian view of convective sources for transport of air across the Tropical Tropopause Layer: distribution, times and the radiative influence of clouds, Atmos. Chem. Phys., 11, 12517–12534, doi:10.5194/acp-11-12517-2011, 2011.

Vernier, J. P., Thomason, L. W., and Karl, J.: CALIPSO detection of an Asian tropopause aerosol layer, Geophys. Res. Lett., 38, L07804, https://doi.org/10.1029/2010GL046614, 2011.

Vernier, J., et al.: BATAL: the balloon measurement campaigns of the Asian Tropopause aerosol layer. Bull. Am. Meteorol. Soc. 0. https://doi.org/10.1175/BAMS-D-17-0014.1, 2017.

Vogel, B., Günther, G., Müller, R., Grooß, J.-U., Afchine, A., Bozem, H., Hoor, P., Krämer, M., Müller, S., Riese, M., Rolf, C., Spelten, N., Stiller, G. P., Ungermann, J., and Zahn, A.: Longrange transport pathways of tropospheric source gases originating in Asia into the northern lower stratosphere during the Asian monsoon season 2012, Atmos. Chem. Phys., 16, 15301–15325, https://doi.org/10.5194/acp-16-15301-2016, 2016.

Winker, D. M., Vaughan, M. A., Omar, A., Hu, Y. X., Powell, K. A., Liu, Z. Y., Hunt, W. H., and Young, S. A.: Overview of the CALIPSO Mission and CALIOP Data Processing Algorithms, J. Atmos. Ocean. Tech., 26, 2310–2323, doi:10.1175/2009jtecha1281.1, 2009.

Wu, G., Liu, Y., Dong, B., Liang, X., Duan, A., Bao, Q., and Yu, J.: Revisiting Asian monsoon formation and change associated with Tibetan Plateau forcing: I. Formation, Climate Dyn., 39, 1169–1181, https://doi.org/10.1007/s00382-012-1334-z, 2012.

Wright, J. S., Fu, R., Fueglistaler, S., Liu, Y. S., and Zhang, Y.: The influence of summertime convection over Southeast Asia on water vapor in the tropical stratosphere, J. Geophys. Res., 116, D12302, doi:10.1029/2010JD015416, 2011.

Yuan, C., Lau, W. K. M., Li, Z., and Cribb, M.: Relationship between Asian monsoon strength and transport of surface aerosols to the Asian Tropopause Aerosol Layer (ATAL): interannual variability and decadal changes, Atmos. Chem. Phys., 19, 1901-1913, https://doi.org/10.5194/acp-19-1901-2019, 2019.

https://doi.org/10.5194/acp-2019-743
Preprint. Discussion started: 2 December 2019

Atmospheric Chemistry and Physics Discussions
Open Access
EGU

Figures

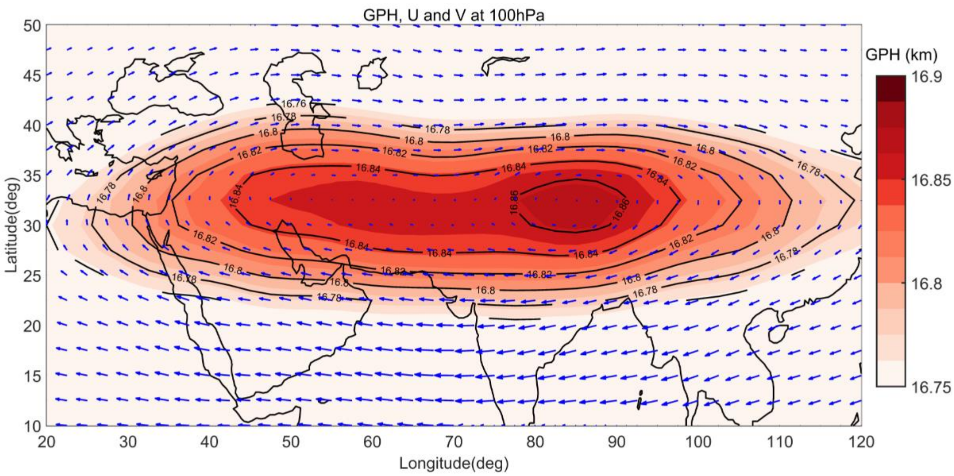

Figure 1. Climatology of GPH superimposed with wind vectors at 100 hPa from NCEP/NCAR reanalysis data during July and August months averaged from the year 2006-2016. The area with GPH values ranging from 16.75-16.9 km are considered as anticyclone region.

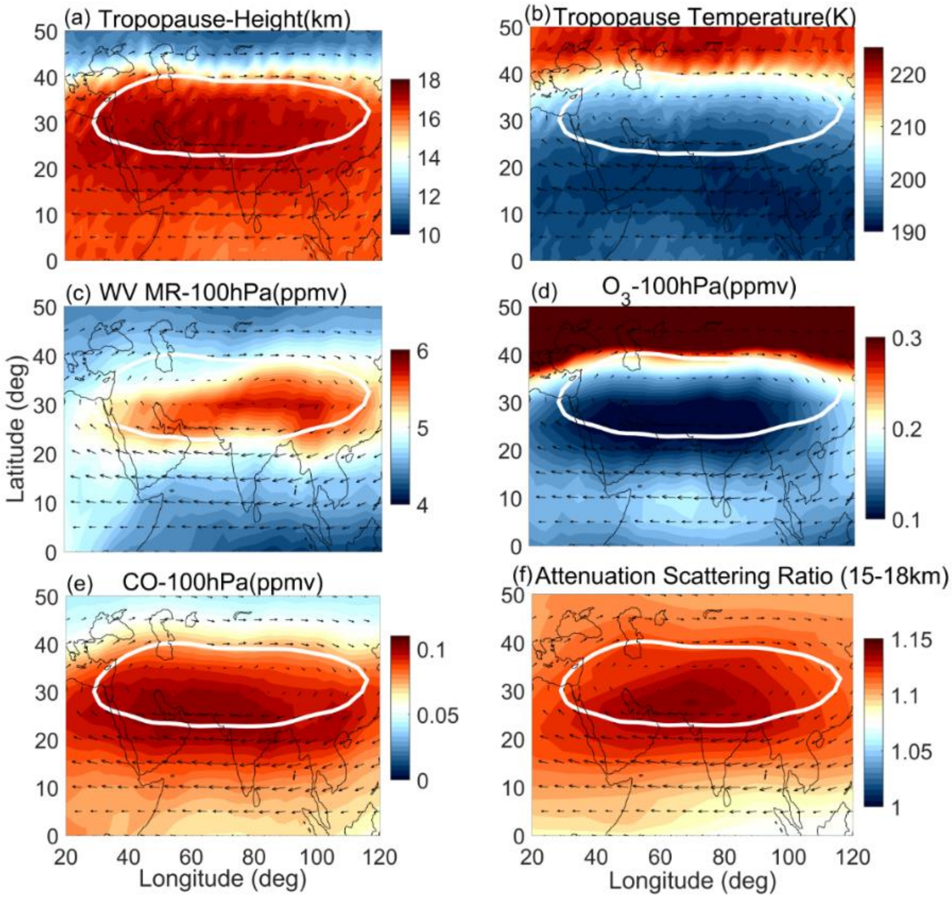

Figure 2. Spatial distribution of (a) tropopause altitude and (b) tropopause temperature obtained from COSMIC satellite observations, (c)WVMR, (d) O_3, and (e) CO obtained from MLS satellite observations at 100 hPa and (f) ASR obtained from CALIPSO stratospheric aerosol product averaged between 16.5-18.5 km altitudes. All the data sets were obtained during July and August months and superimposed with wind vectors of 100 hPa obtained from NCEP/NCAR reanalysis data during 2006-2016. The white line indicates the GPH contour line at 16.75 km which represents the anticyclone.

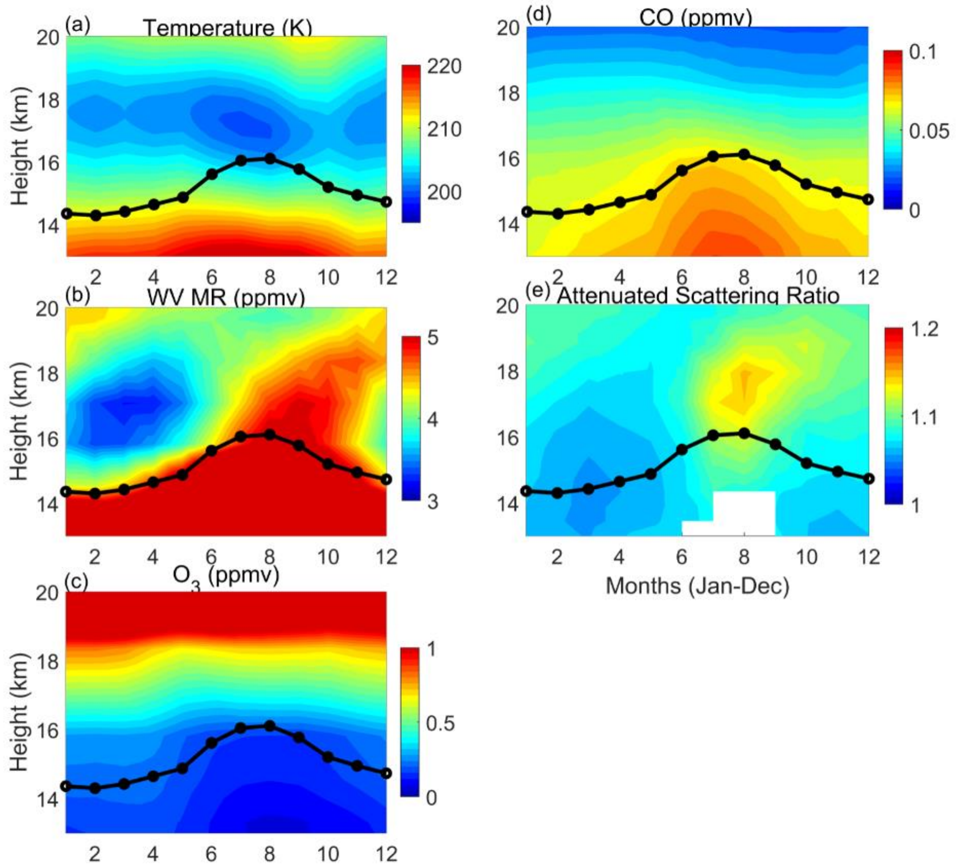

Figure 3. Monthly mean climatology of (a) temperature obtained from COSMIC, (b) WVMR, (c) O_3,(d) CO obtained from MLS observations, and (e) ASR obtained from CALIPSO stratospheric aerosol product averaged in the grid 30°E-110°E longitude and 22.5°N-40°N latitude from 2006-2016. The black line denotes the tropopause altitude derived from COSMIC satellite data during the same period.

Atmospheric Chemistry and Physics
Open Access
Discussions

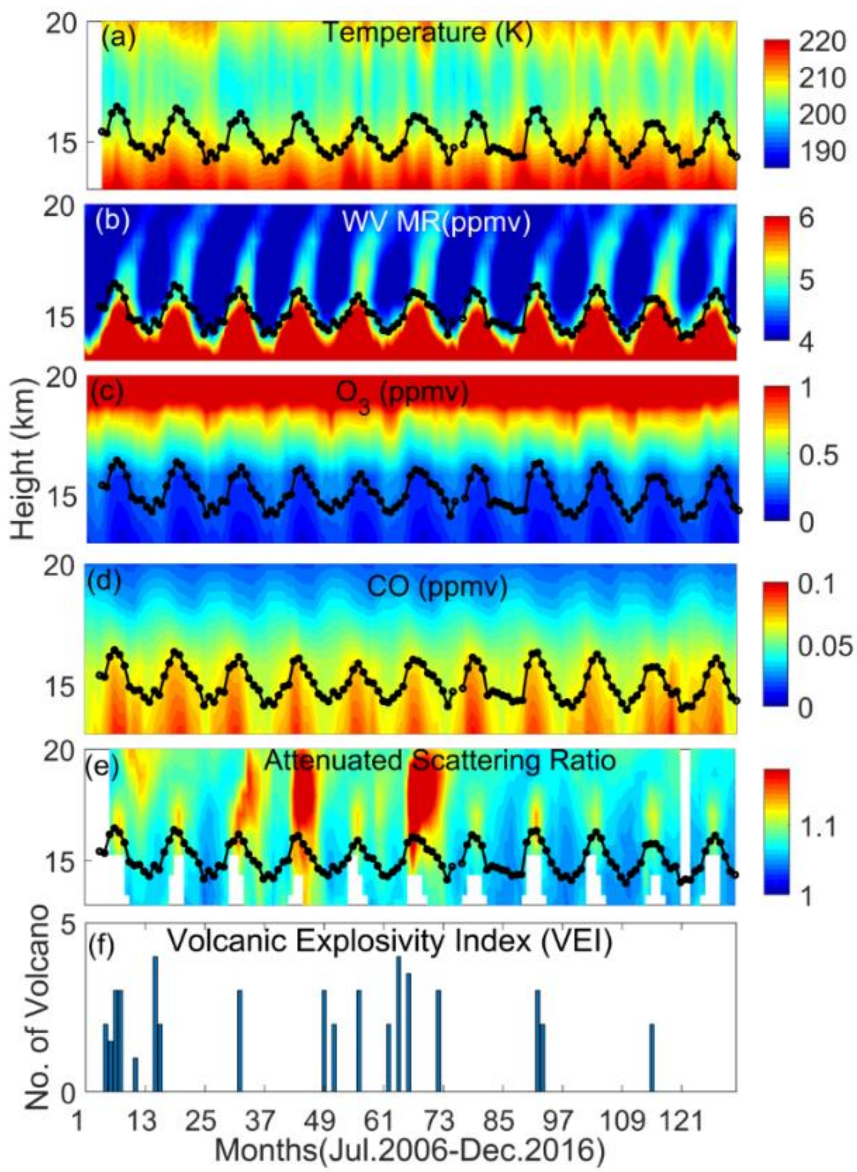

Figure 4. Inter-annual variation observed in (a) temperature obtained from COSMIC, (b) WVMR, (c) O_3, (d) CO obtained from MLS observations, and (e) ASR obtained from CALIPSO stratospheric aerosol product d averaged in the grid 30°E-110° E longitude and 22.5°N-40°N latitude from 2006-2016. (f) Volcanic explosivity index. The black line denotes tropopause altitude derived from COSMIC satellite measurements.

https://doi.org/10.5194/acp-2019-743
Preprint. Discussion started: 2 December 2019

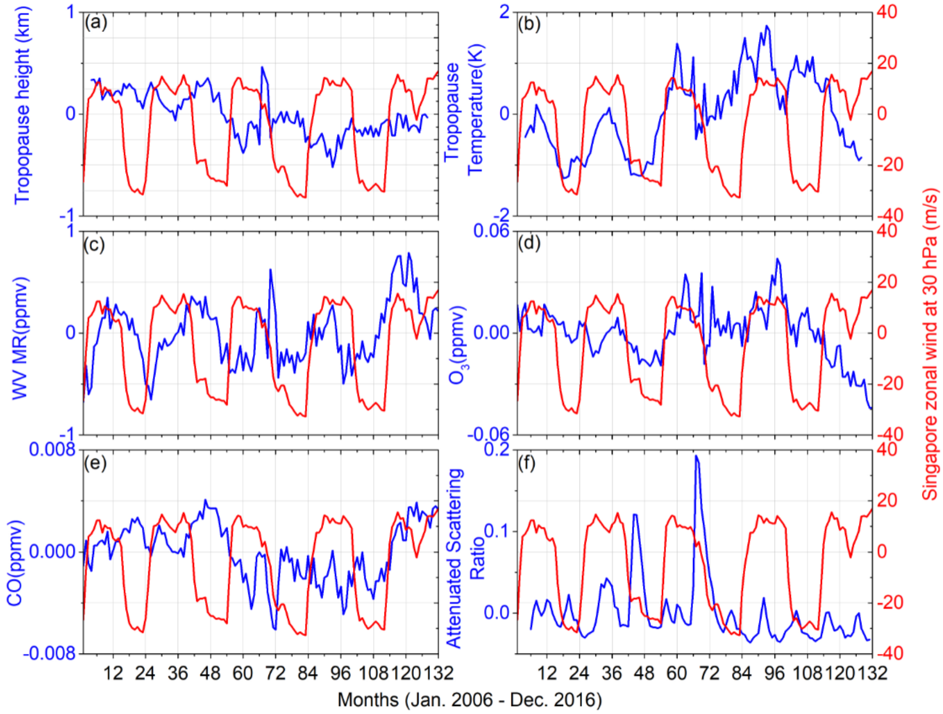

Figure 5. Time series of deseasonalized (a) tropopause altitude, (b) tropopause temperature obtained from COSMIC, (c) WVMR, (d) O_3, (e) CO at 100 hPa obtained from MLS satellite observations and (e) ASR obtained from CALIPSO (16-18 km averaged) with multivariate linear regression based on QBO proxies in ASMA region from 2006 to 2016. The resulting fits are shown here (blue line). The QBO (Singapore zonal wind data at 30 hPa) variability is also shown (red line).

https://doi.org/10.5194/acp-2019-743
Preprint. Discussion started: 2 December 2019

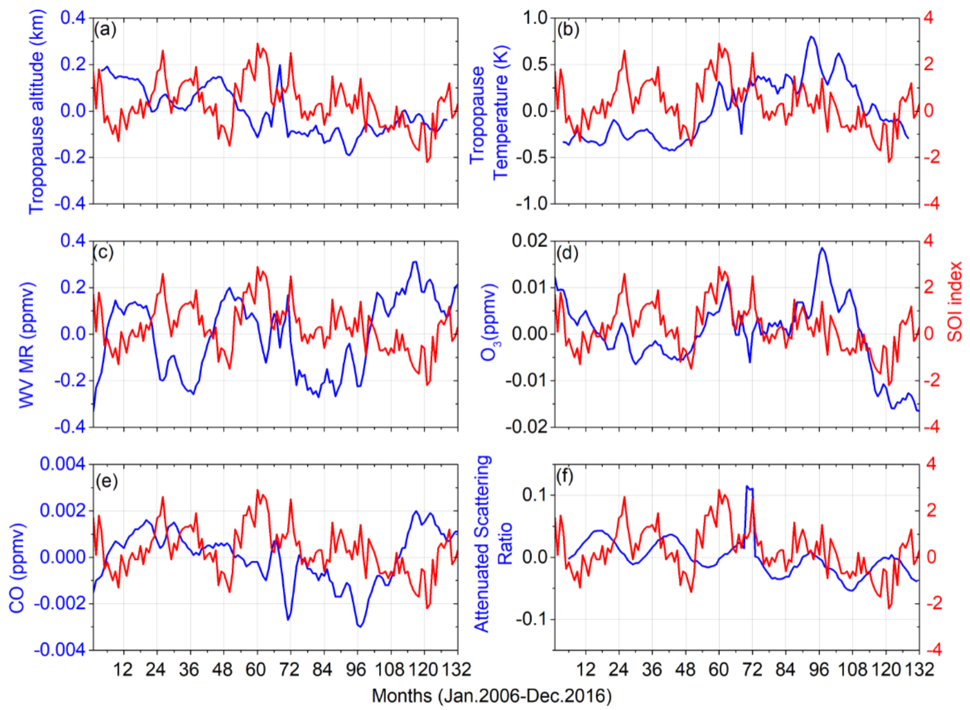

Figure 6. Time series of deseasonalized (a) tropopause altitude, (b) tropopause temperature obtained from COSMIC, (c) WVMR, (d) O_3, (e) CO at 100 hPa obtained from MLS satellite observations and (e) ASR obtained from CALIPSO (16-18 km averaged) with multivariate linear regression based on ENSO proxies in ASMA region from 2006 to 2016. The resulting fits are shown here (blue line). The Southern Oscillation Index (SOI) is also shown (red line).

https://doi.org/10.5194/acp-2019-743
Preprint. Discussion started: 2 December 2019

Atmospheric Chemistry and Physics
Discussions

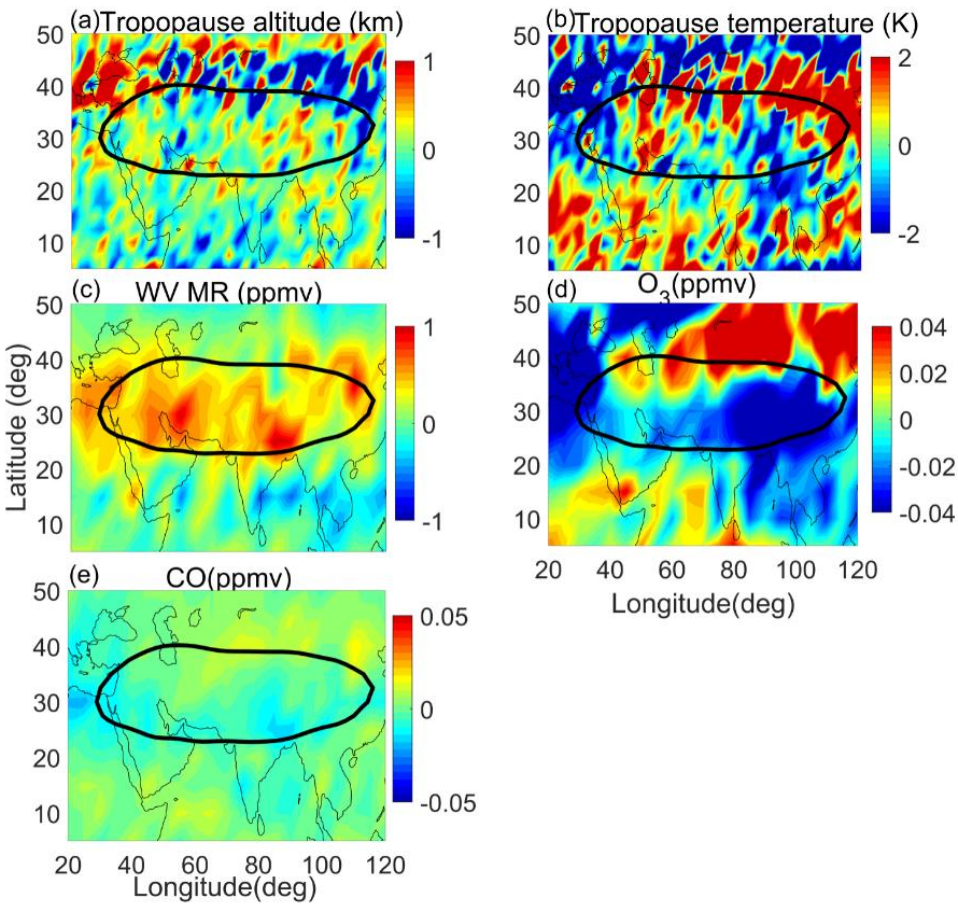

650

651 Figure 7. Spatial mean difference between active and break spells observed in (a) tropopause altitude (km), (b) tropopause temperature (K) from COSMIC GPSRO measurements, (c) WVMR (ppmv), (d) O_3 (ppmv), and (e) CO (ppmv) obtained from MLS observations from 2006 to 2016 at 100 hPa. Black line denotes the GPH at 16.75km which represents the core of the anticyclone.

https://doi.org/10.5194/acp-2019-743
Preprint. Discussion started: 2 December 2019

Atmospheric Chemistry and Physics
Open Access
Discussions

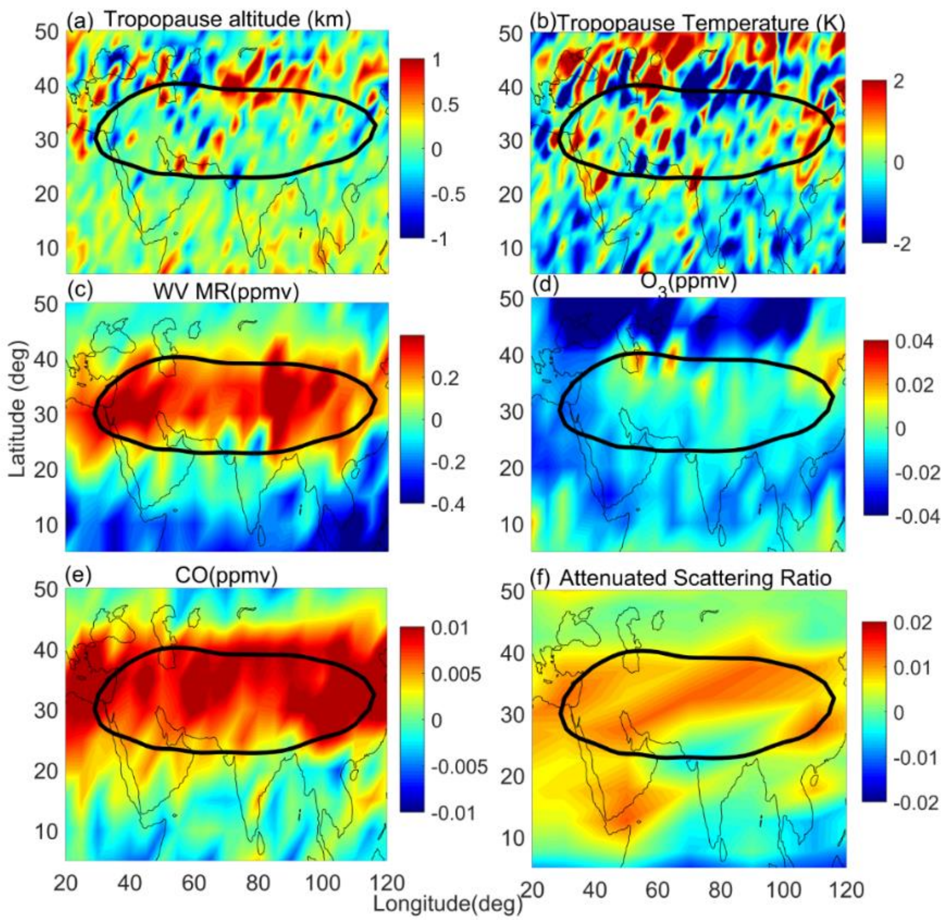

Figure 8. Spatial mean difference between strong and weak monsoon years in (a) tropopause altitude (km), (b) tropopause temperature (K) from COSMIC GPSRO measurements, (c) WVMR (ppmv), (d) O_3 (ppmv), and (e) CO (ppmv) obtained from MLS observations at 100 hPa, (f) ASR obtained from CALIPSO stratospheric Aerosol product averaged between 16-18 km from 2006 to 2016 at 100 hPa. Black line denotes the GPH at 16.75km which represents the core of the anticyclone.

https://doi.org/10.5194/acp-2019-743
Preprint. Discussion started: 2 December 2019

Atmospheric Chemistry and Physics Discussions

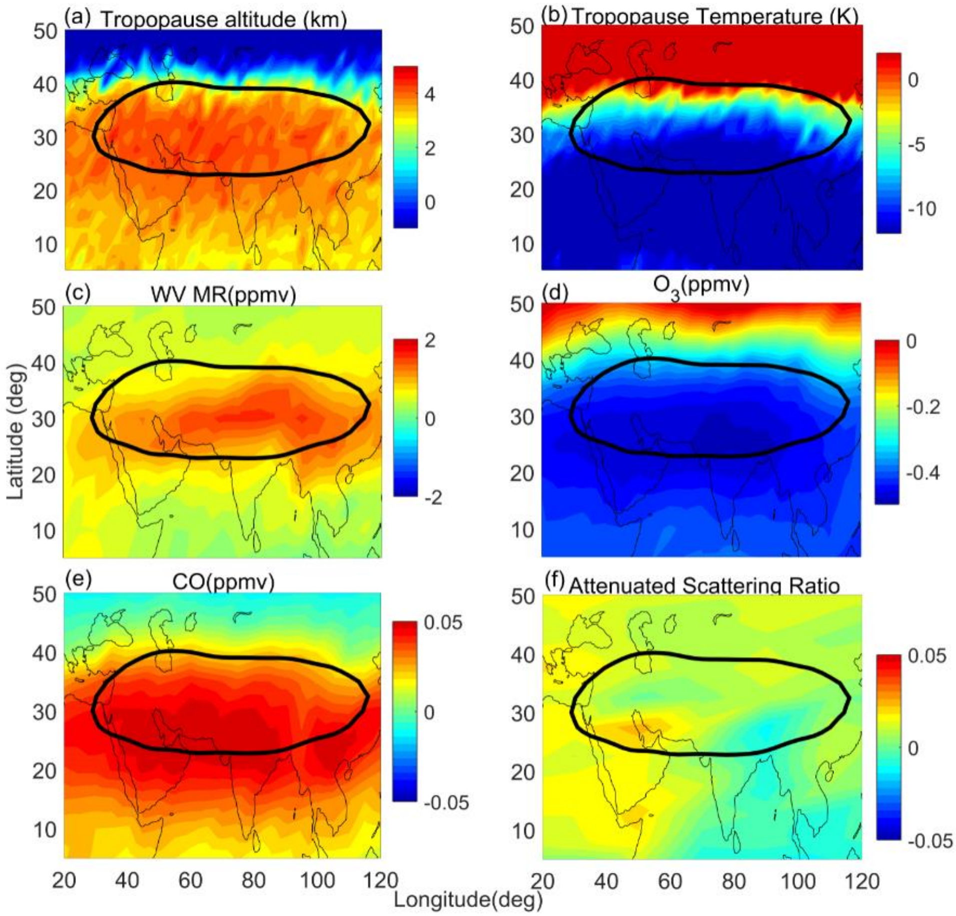

Figure 9. Spatial mean difference between La Niña and El Niño in (a) tropopause altitude (km), (b) tropopause temperature (K) from COSMIC GPSRO measurements, (c) WVMR (ppmv), (d) O_3 (ppmv), and (e) CO (ppmv) obtained from MLS observations at 100 hPa, (f) ASR obtained from CALIPSO stratospheric Aerosol product averaged between 16-18 km from 2006 to 2016 at 100 hPa. Black line denotes the GPH at 16.75km which represents the core of the anticyclone.